
RanDeS: Randomized Delta Superposition for Multi-Model Compression

Hangyu Zhou, Aaron Gokaslan, Volodymyr Kuleshov, Bharath Hariharan
Computer Science, Cornell University
{hz477, ak87, vk379, bh497}@cornell.edu
<https://github.com/Zhou-Hangyu/randes>

Abstract

From a multi-model compression perspective, model merging enables memory-efficient serving of multiple models fine-tuned from the same base, but suffers from degraded performance due to interference among their task-specific parameter adjustments (i.e., deltas). In this paper, we reformulate model merging as a compress-and-retrieve scheme, revealing that the task interference arises from the summation of irrelevant deltas during model retrieval. To address this issue, we use random orthogonal transformations to decorrelate these vectors into self-cancellation. We show that this approach drastically reduces interference, improving performance across both vision and language tasks. Since these transformations are fully defined by random seeds, adding new models requires no extra memory. Further, their data- and model-agnostic nature enables easy addition or removal of models with minimal compute overhead, supporting efficient and flexible multi-model serving.

1 Introduction

Contemporary advances in machine learning are fueled by ever larger models trained on massive datasets [Villalobos et al., 2022]. This leads to a blossom of fine-tuned models specialized for individual tasks and users’ needs. As the number of fine-tuned models proliferates, the memory cost of serving them becomes substantial. Compressing models with off-the-shelf tools provides a straight-forward solution, but fails to leverage the parameter redundancy between fine-tuned models with the same base [Anwar et al., 2017, Liao et al., 2023, Gholami et al., 2022, Gou et al., 2021, Yu et al., 2017]. Delta compression alleviates this issue by decomposing fine-tuned model parameters into their pre-trained components and *deltas* (parameter differences between the fine-tuned model and their base models), and only compressing individual deltas [Liu et al., 2024, Ping et al., 2024]. But the redundancy between deltas is still left unexplored. At the other extreme, model merging treats all task-specific adjustments as redundant and proposes to reduce all models down to a single set of weights [Wortsman et al., 2022, Ilharco et al., 2022]. But various studies [Yadav et al., 2024, Wang et al., 2024, Ortiz-Jimenez et al., 2024] have shown that the interference between different models, which grows more prominent with more merged models, leads to significant performance drops.

In this paper, we take a renewed look at model merging and find that for a specific task, the cause of interference are the merged deltas for the other tasks. Armed with this insight, we propose a simple framework for interference reduction with no training and minimal memory overhead. We dub our framework *Randomized Delta Superposition (RanDeS)*, as it works by superposing deltas with conflicting deltas randomly decorrelated into self-cancellation. Thanks to the high dimensionality of modern neural networks, we can induce orthogonality among deltas using random transformations without training. Being random also allows for specifying highly-complex transformations with

memory-efficient random seeds. These features make *RanDeS* preferable for multi-model serving settings with resource restrictions and dynamic user requests.

We substantiate *RanDeS* with two efficient layer-wise implementations. Our first approach is to *shuffle* each delta’s layers before combining them, with an inverse shuffling applied at test time. Our second approach is to apply a *random column-wise sign flip* or *reflection* to each layer of the deltas before merging them, again inverting the transformation at test time. We test these approaches on three multi-model serving benchmarks with different use cases: up to 20 CLIP-ViT-B/32 and ViT-L/14 models for zero-shot image classification [Radford et al., 2021], 8 Flan-T5-base models (along with LoRA [Hu et al., 2021] variants) for text generation [Longpre et al., 2023], and 7 GPT-2 for text classification [Radford et al., 2019]. We find that across all of these benchmarks, our approach substantially improves in terms of accuracy over prior model merging-based approaches. When compared to the original fine-tuned models, in two of the three benchmarks our approach yields near-identical accuracy to the individual models while reducing the storage costs by $4\times$.

2 Problem setup

We are given T models $\{\Theta_i \in \mathbb{R}^d\}_{i=1}^T$ fine-tuned from a pre-trained model $\Theta_0 \in \mathbb{R}^d$ on tasks $i = 1, \dots, T$. Our goal is to compress $\{\Theta_i\}_{i=1}^T$ into a compact representation $\Theta_* = \text{compress}(\{\Theta_i\}_{i=1}^T)$ with minimal memory usage, so that at test time, given a task i , we can retrieve an *approximate* model $\hat{\Theta}_i = \text{retrieve}(\Theta_*, i)$ for the task i that achieves high accuracy.

3 Interference in Model Merging

Model merging approaches the problem by merging T models into a single model with performance degradation due to task interference [Wortsman et al., 2022, Ilharco et al., 2022, Yadav et al., 2024, Wang et al., 2024, Ortiz-Jimenez et al., 2024]. Here we use *task arithmetic* [Ilharco et al., 2022], a popular model merging framework, as an example to show what is interference and how to reduce it. The same analysis applies to other common frameworks.

Task arithmetic starts with decomposing each model Θ_i into its pre-trained model, Θ_0 , and the weight delta $\Delta_i = \Theta_i - \Theta_0$ (also known as *task vector*). Then individual deltas are aggregated before merging back to the shared pre-trained model weights:

$$\Theta_*^{TA} \leftarrow \Theta_0 + \lambda \sum_{i=1}^T \Delta_i, \quad (1)$$

where $\lambda \in \mathbb{R}^+$ is the scaling coefficient. At test time, this compressed model is directly applied no matter what the task:

$$\begin{aligned} \hat{\Theta}_i^{TA} &\leftarrow \Theta_*^{TA}, \\ &= \Theta_0 + \lambda \sum_{i=1}^T (\Theta_i - \Theta_0), \\ &= (1 - \lambda)\Theta_0 + \lambda\Theta_i + \lambda \sum_{j \neq i} \Delta_j. \end{aligned} \quad (2)$$

The last line suggests the model being applied to task i is interpolating between the pre-trained model Θ_0 and the fine-tuned model Θ_i , but with interference coming from other merged deltas: $\lambda \sum_{j \neq i} \Delta_j$. To retrieve Θ_i , the first two terms suggest that we should set λ to 1. However this will inevitably *increase* the interference. Some prior work has tried to achieve a good balance by optimizing λ for each model and layer using test-time adaptation [Yang et al., 2023], but performance drop still persists.

Instead of juggling with λ , we directly suppressing interference by reducing its l_2 norm:

$$\left\| \lambda \sum_{j \neq i} \Delta_j \right\| = \lambda \sqrt{\sum_{j \neq i} \|\Delta_j\|_2^2 + 2 \sum_{\substack{1 \leq l < j \leq n \\ l, j \neq i}} \|\Delta_l\|_2 \|\Delta_j\|_2 \cos(\Delta_l, \Delta_j)}. \quad (3)$$

We observe that the magnitude of interference is negatively correlated with the cosine similarity between deltas. This means we can reduce interference by decorrelating the conflicting deltas $\{\Delta_j\}_{j \neq i}$ without altering Δ_i . Below, we propose *Randomized Delta Superposition (RanDeS)* as a principled framework for doing this.

4 Randomized Delta Superposition (RanDeS)

At a high level, *RanDeS* first randomizes the deltas with random orthogonal transformations before merging, which decorrelates the deltas due to high dimensionality. At test time, each delta can be retrieved with its inverse orthogonal transformation while preserving the pairwise orthogonality among conflicting deltas.

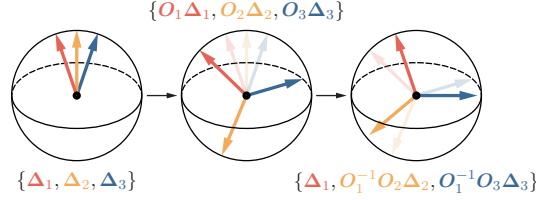


Figure 1: Illustration of *RanDeS* with three deltas $\{\Delta_i\}_{i=1}^3$.

Concretely, given T fine-tuned models $\{\Theta_i \in \mathbb{R}^d\}_{i=1}^T$ and the pre-trained model $\Theta_0 \in \mathbb{R}^d$, we first derive the deltas $\{\Delta_i \in \mathbb{R}^d\}_{i=1}^T$. Then we transform each delta Δ_i with an orthogonal transformation O_i sampled from the orthogonal group $\mathbb{O}(d)$ before merging back to the shared pre-trained model weights:

$$\Theta_*^{RanDeS} \leftarrow \Theta_0 + \lambda \sum_{i=1}^T O_i \Delta_i, \quad (4)$$

$$\forall i. O_i \sim \mathbb{O}(d). \quad (5)$$

where $\lambda \in \mathbb{R}^+$ is the scaling coefficient. At test time, given task i , we retrieve an approximate model $\hat{\Theta}_i$ with:

$$\begin{aligned} \hat{\Theta}_i^{RanDeS} &\leftarrow \Theta_0 + \lambda O_i^{-1} \sum_{i=1}^T O_i \Delta_i, \\ &= (1 - \lambda) \Theta_0 + \lambda \Theta_i + \lambda \sum_{j \neq i} O_i^{-1} O_j \Delta_j. \end{aligned} \quad (6)$$

Figure 1 shows how *RanDeS* works in action with three models.

4.1 Implication

RanDeS provides a principled framework to reduce interference by decorrelating conflicting deltas into self-cancellation without changing the delta in request. Comparing to model merging [Ilharco et al., 2022], *RanDeS* doubles memory footprint to enable task-specific delta retrieval. But it requires effectively *zero* memory overhead to compress more models after the initial setup, since each random orthogonal transformation O_i can be specified with a random seed. Thus we can reach higher compression ratio when more models are superposed together.

However, it is impractical to sample the orthogonal transformations directly due to their $O(d^2)$ complexity. We propose two layer-wise implementation to solve this problem: *layer shuffling* and *layer column-wise random sign flips*.

4.2 Layer-wise Notation

Each model Θ_i is a set of parameter matrices:

$$\Theta_i = \left\{ \mathbb{I}_i, \left(M_i^{k,1}, M_i^{k,2}, \dots, M_i^{k,m_k} \right)_{k=1}^K, \mathbb{O}_i \right\}.$$

Here \mathbb{I}_i and \mathbb{O}_i are the input and output layers. Each model has K blocks, with the k -th block containing m_k matrices $M_i^{k,1}, M_i^{k,2}, \dots, M_i^{k,m_k}$. We use $\Delta_i^{k,1}, \Delta_i^{k,2}, \dots, \Delta_i^{k,m_k}$ to denote the corresponding delta matrices.

4.3 Layer Shuffling

Across several model architectures (CLIP-ViT-B/32 [Radford et al., 2021], Flan-T5 [Longpre et al., 2023], and GPT-2 [Radford et al., 2019]), we observed that delta layers within the same model exhibit greater variability compared to corresponding layers across fine-tuned models (see Figure 2).

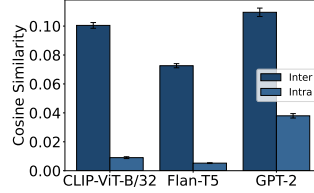


Figure 2: Cosine similarity distributions between delta layers within and across models for CLIP-ViT-B/32, Flan-T5, and GPT-2.

This suggests that we can decorrelate deltas by shuffling layers within each delta. Leveraging the repeating structure in modern neural networks, for each delta, we *randomly permute* within layers of the same type (e.g., $\{\Delta_i^{k,j}\}_{k=1}^K$) to avoid size mismatches. Concretely, for each set of layers $\{\Delta_i^{k,j}\}_{k=1}^K$ within each delta Δ_i , we draw a random permutation $\sigma_i^j \sim \mathbb{S}_K$ from the symmetric group \mathbb{S}_K to shuffle them:

$$\Delta_i^{k,j} \leftarrow \Delta_i^{\sigma_i^j(k),j}, \quad (7)$$

$$\Delta_i^{Shuffle} = P_i \Delta_i. \quad (8)$$

Then, when we want to perform inference using model Θ_i , we perform the inverse of the corresponding permutation to obtain the model. We dub this approach *layer shuffling (RandE-S)*. It implements the orthogonal transformation O_i as a permutation P_i , which can be implemented efficiently by reallocating the pointer to each layer.

4.4 Layer Column-wise Random Sign Flips

We take inspiration from Cheung et al. [2019] on continual learning and introduce *layer column-wise random sign flips (RandE-S-RSF)* as another memory-efficient implementation for the random orthogonal transformations.

Considering merging layer $\Delta^{k,j}$ across deltas: $\{\Delta_i^{k,j} \in \mathbb{R}^{m,n}\}_{i=1}^T$, we sample random binary diagonal matrices (*context matrices*) whose diagonal entries have equal probability to be +1 or -1 to each of the T matrices and apply them before summation:

$$\Delta_*^{k,j} \leftarrow \sum_{i=1}^T \Delta_i^{k,j} D_i^{k,j}. \quad (9)$$

When performing task i , we apply the layer-wise inverse transformation $D_i^{k,j(-1)}$ to retrieve the delta layer $\Delta_i^{k,j}$ from the superposition:

$$\hat{\Delta}_i^{k,j} = \Delta_*^{k,j} D_i^{k,j(-1)}, \quad (10)$$

$$= \Delta_i^{k,j} + \sum_{l \neq i} [\Delta_l^{k,j} D_l^{k,j} D_i^{k,j(-1)}]. \quad (11)$$

We name this method *layer column-wise random sign flips*, as it decorrelates deltas by randomly flipping the sign for each column. Since $n \ll d$, the layer-wise transformations $\{D_i^{k,j}\}_{k,j}$ requires far less memory footprint comparing to the orthogonal transformation O_i .

5 Experiments

We evaluate *RanDeS* across vision and language tasks, showing comparable performance for discriminative and generative models, as well as PEFT models. Through ablation studies, we analyze component importance, merging coefficient effects, and context matrix designs.

5.1 Experiment Setup

	Original			RanDeS-S			RanDeS-RSF			RanDeS-SRSF		
SUN397	1.0000	0.0221	0.0289	1.0000	0.0043	0.0027	1.0000	0.0007	0.0008	1.0000	0.0002	-0.0000
Cars	0.0221	1.0000	0.0182	0.0043	1.0000	0.0035	0.0007	1.0000	0.0001	0.0002	1.0000	0.0000
RESISC45	0.0289	0.0182	1.0000	0.0027	0.0035	1.0000	0.0008	0.0001	1.0000	-0.0000	0.0000	1.0000
	SUN397	Cars	RESISC45	SUN397	Cars	RESISC45	SUN397	Cars	RESISC45	SUN397	Cars	RESISC45

Figure 3: Average pairwise cosine similarity of three out of eight CLIP-ViT-B/32 task vectors during model retrieval for SUN397 across three repetitions. Both *RanDeS-S* and *RanDeS-RSF* increase mutual orthogonality, with an additive effect when combined.

Datasets and Models. We follow Tang et al. [2024a] and select three representative scenarios to evaluate our methods. This includes i) CLIP-ViT-B/32 fine-tuned on eight image classification datasets (adopted from [Ilharco et al., 2022]); ii) Flan-T5-base fine-tuned on eight text generation datasets; and iii) GPT-2 fine-tuned on seven text classification datasets. Detailed information on the datasets and models is in Appendix B.

Baselines and Metrics. We evaluate baselines from model merging/compression literature, grouped by memory requirements: methods using the original footprint (pre-trained model, standard merging techniques) and those requiring additional memory (fine-tuned models, newer merging baselines). The pre-trained and fine-tuned models provide lower and upper performance bounds respectively. Following Ilharco et al. [2022], we optimize merging coefficient λ via validation set grid search. We report accuracy and memory usage across three runs per experiment with random operations. See Appendix B for details.

5.2 Performance Analysis

Table 1: Performance and memory comparison of CLIP-ViT-B/32 models across eight image classification tasks, showing absolute and normalized accuracy (%), as well as memory footprint (Gb). Results averaged over three runs where applicable. Variances smaller than 0.1% are omitted.

Method	Avg.(%) \uparrow	Bits(Gb) \downarrow	SUN397	Cars	RESISC45	EuroSAT	SVHN	GTSRB	MNIST	DTD
Pre-trained	48.2 (53.4)	0.564 (1.00)	63.2	59.8	60.7	46.0	31.6	32.5	48.3	43.9
Weight Averaging	66.5 (73.6)	0.564 (1.00)	65.4	62.6	70.8	76.9	64.5	54.9	86.3	50.9
Fisher Merging	70.6 (78.2)	0.564 (1.00)	66.7	64.0	72.2	91.6	69.0	64.3	83.5	53.7
RegMean	80.5 (89.1)	0.564 (1.00)	67.8	68.9	82.5	94.4	90.6	79.2	94.7	63.2
Task Arithmetic	69.8 (77.2)	0.564 (1.00)	64.4	61.5	70.5	80.4	73.9	62.8	93.0	51.6
Ties-Merging	72.2 (80.0)	0.564 (1.00)	67.1	64.2	74.1	91.6	77.7	69.4	94.1	54.0
Layerwise AdaMerging	82.6 (91.5)	0.564 (1.00)	67.9	71.3	83.5	92.7	87.4	92.9	98.2	67.0
Fine-tuned	90.3 (100)	2.84 (5.03)	75.0	78.3	95.2	99.0	97.3	98.9	99.6	79.7
WEMoE	89.2 (98.8)	2.27 (4.03)	73.7	76.8	93.4	98.2	96.8	98.2	99.6	76.6
SMILE	89.3 (98.9)	1.23 (2.20)	73.6	77.8	92.0	<u>98.3</u>	96.9	98.1	99.6	<u>78.1</u>
RanDeS-S (Ours)	81.3 (90.0)	0.89 (1.58)	65.6	58.5	86.8	<u>94.5</u>	93.2	91.4	98.5	62.2
RanDeS-RSF (Ours)	89.6 (<u>92.2</u>)	0.89 (1.58)	<u>74.4</u>	75.6	<u>94.6</u>	99.0	<u>97.1</u>	<u>98.5</u>	<u>99.5</u>	77.8
RanDeS-SRSF (Ours)	89.9 (99.6)	0.89 (1.58)	74.8	76.7	94.8	99.0	97.2	98.6	<u>99.5</u>	78.7

Superior MTL Performance. Our approach achieves significant accuracy gains across benchmarks (Tables 1, 2 and 6), with *RanDeS-SRSF* nearly matching individual fine-tuned models. We outperform WEMoE [Tang et al., 2024c] and SMILE [Tang et al., 2024b] on image classification while using

Table 2: Performance and memory comparison of Flan-T5-base models across eight GLUE text generation tasks, showing absolute and normalized accuracy (%), as well as memory footprint (Gb). Results averaged over three runs where applicable. Variances smaller than 0.1% are omitted.

Method	Avg.(%) \uparrow	Bits(Gb) \downarrow	CoLA	MNLI	MRPC	QNLI	QQP	RTE	SST2	STSB
Pre-trained	75.7 (87.6)	1.19 (1.00)	69.1	56.5	76.2	88.4	82.1	80.1	91.2	62.2
Weight Averaging	78.9 (91.3)	1.19 (1.00)	69.1	62.6	79.4	89.8	83.9	81.2	91.7	73.2
Task Arithmetic	79.6 (92.1)	1.19 (1.00)	69.7	64.1	79.2	90.2	83.9	81.6	92.1	76.4
Ties-Merging	79.9 (92.5)	1.19 (1.00)	70.3	65.0	78.9	90.2	83.5	81.6	91.7	78.3
Fine-tuned	86.4 (100)	9.52 (8.00)	75.0	83.4	87.5	91.5	85.4	85.9	93.6	88.7
SMILE	85.5 (99.0)	1.81 (1.52)	73.2	84.2	85.0	91.3	84.9	84.8	<u>93.5</u>	87.3
RanDeS-S (Ours)	85.7 (99.0)	2.38 (2.00)	75.5	82.0	87.5	91.1	83.9	83.8	93.6	88.4
RanDeS-RSF (Ours)	86.5 (100)	2.38 (2.00)	77.2	82.1	87.6	<u>91.6</u>	85.3	85.7	93.2	89.0
RanDeS-SRSF (Ours)	<u>86.4</u> (100)	2.38 (2.00)	<u>75.6</u>	<u>82.8</u>	88.2	91.7	85.3	85.7	<u>93.5</u>	<u>88.9</u>

only 40% and 72% of their respective memory footprints, and surpass SMILE’s text generation performance at benchmark saturation. Though Task Arithmetic [Ilharco et al., 2022] uses 55% of our storage, its performance is substantially lower.

Amortizable Memory Overhead. Our method requires only 2x memory, mainly from storing the delta superposition. By storing random seeds and regenerating transformations on-the-fly with minimal overhead (292.70 ms for CLIP-ViT-B/32, 658.19 ms for CLIP-ViT-L/14 on Intel Xeon Gold 6448Y CPU), we achieve effectively zero additional memory per model. This enables efficient scaling, demonstrated by merging 20 CLIP-ViT-L/14 models with state-of-the-art performance and 9x memory reduction (Sec. 5.9).

5.3 Key Components Ablation

In this section, we ablate both the *layer shuffling* and *layer column-wise random sign flips* to show their individual contribution.

As shown in Tables 1, 2, 4, 5 and 6, both methods significantly outperform task arithmetic consistently. In some benchmarks, shuffling works better (Flan-T5-base and GPT-2) while random sign flips works better in others (CLIP). This difference may be because of the nature of deltas themselves: how they vary across the model layers and across different models. We find that the combined approach is able to combine gains from both components, yielding consistently the best result across all the benchmarks. This complementary effect is further manifested in Figure 3, where introducing both mechanism gets the smallest pairwise cosine similarity among interfering deltas. We provide a more detailed analysis of the interplay between shuffling and random sign flips in Section C.

5.4 Impact of Merging Coefficient λ

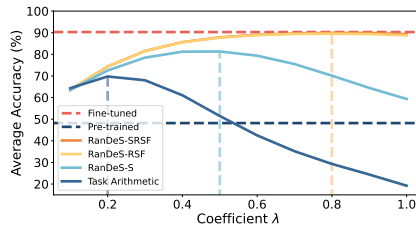


Figure 4: The impact of λ on average accuracy over eight image classification tasks.

Here we examine the interplay between the merging coefficient λ and the average performance across different setup. For each variant, we perform a grid search on $\lambda = \{0.1, 0.2, \dots, 1.0\}$ when compressing eight CLIP-ViT-B/32 models for image classification. Figure 4 shows the change of optimal model performance and the coefficient λ when *layer shuffling* and *column-wise random sign flips* are introduced to task arithmetic.

We observe that when shuffling and random sign flips are introduced, the best performance increases along with the value of λ . This shows the effectiveness of our method in reducing interference, allowing larger λ to be selected for more authentic model retrieval.

5.5 Impact of Context Matrix Design

To further examine how *RanDeS-RSF* works and shed light on better context matrix design, we make a comparison between three types of context matrices: random binary diagonal matrix with $\{-1, +1\}$ entries (RBD), identity matrix (Identity), and random diagonal matrix with entries draw from Normal distribution (RD). We use random layer shuffling when compressing the 8 CLIP-ViT-B/32 models on the image classification tasks.

The average accuracy and its variance with the optimal merging coefficient is shown in Figure 5(a). RBD receives higher accuracy than Identity due to the randomness it introduces, which reduces interference. Despite being random, RD’s accuracy is much lower than RBD. We think this happens because RD is not an orthogonal matrix. It fails to preserve the magnitude and thus disturb this self-cancellation process.

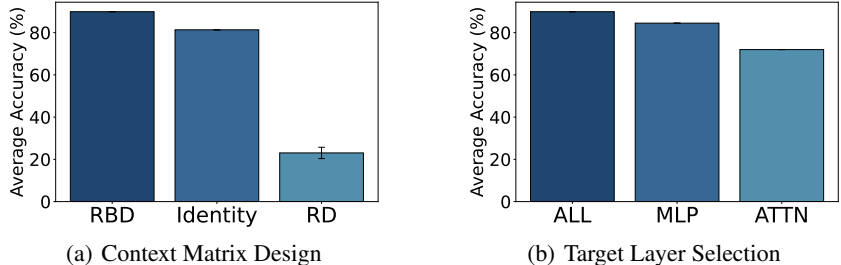


Figure 5: (a) Impact of context matrix design to the average accuracy. RBD stands for random binary diagonal; RD stands for random diagonal. (b) Impact of target layer selection to the average accuracy. ALL stands for choosing all layers; MLP means only MLP layers are selected; and ATTN stands for attention layers.

5.6 Target Layer Selection

By default we apply the random operations on all layers within the models. In this section, we evaluate the benefits of targeting specific types of layers. To do this, we create two variants: MLP (which selects only the MLP layers) and ATTN (which selects only the attention layers), in addition to the default setup (ALL). Figure 5 (b) shows the average accuracy for each setup across eight image classification tasks using CLIP-ViT-B/32. The ALL configuration achieves the highest accuracy, followed by MLP and ATTN. Note that the total number of parameters in MLP is twice that of ATTN, explaining the gradual decline in performance as fewer parameters are selected.

5.7 Model Hot Swapping

The ability to hot-swap models in real-world applications is crucial, especially in dynamic environments like model serving, where new models need to be integrated into the system regularly, and deprecated ones need to be removed in a timely fashion. As mentioned, the *RanDeS-SRSF* method allows for this by shuffling layers and sampling diagonal binary matrices *independently* of data or model parameters, thus enabling the on-the-fly addition of new models without the need for recomputation. This provides a big advantage over methods like WEMoE which require recomputation of the router when new models are added [Tang et al., 2024c], or TALL-masks, which needs to recompute all task masks when a new model is added [Wang et al., 2024].

5.8 Parameter Efficient Finetuning (PEFT) Model Compression

We can also apply our method on PEFT adapter weights. Consider LoRA [Hu et al., 2021], where we have a fixed pre-trained model Θ_0 , along with LoRA weights L_i . We merge the LoRA weights to

Table 3: Comparison of selected methods with hot adding and recomputation requirements when new models are added to the pool.

Method	Hot Swap	Recomputation
Task Arithmetic	✓	✗
WEMoE	✗	✓
TALL-masks	✗	✓
RanDeS-SRSF	✓	✗

get the fine-tuned model: $\Theta_i = \Theta_0 + \lambda L_i$. We apply *layer shuffling* and *random column-wise sign flips* on these LoRA weight vectors before retrieval.

Experiments on Flan-T5-base LoRA fine-tunes [Longpre et al., 2023, Tang et al., 2024a,b] demonstrate that our method is performative in PEFT compression settings as well (Table 4). With 99.8% normalized average accuracy compare to the fine-tuned baseline, and 1.20 Gb memory usage, our method presents a better trade-off point between performance and storage usage than the state-of-the-art model SMILE [Tang et al., 2024b].

Table 4: Performance and memory comparison of Flan-T5-base LoRA models across eight GLUE text generation tasks, showing absolute and normalized accuracy (%), as well as memory footprint (Gb). Results averaged over three runs where applicable. Variances smaller than 0.1% are omitted.

Method	Avg.(%) ↑	Bits(Gb) ↓	CoLA	MNLI	MRPC	QNLI	QQP	RTE	SST2	STSB
Pre-trained	75.7 (87.6)	1.19 (1.00)	69.1	56.5	76.2	88.4	82.1	80.1	91.2	62.2
Weight Averaging	78.2 (92.4)	1.19 (1.00)	69.7	59.7	78.9	90.1	83.8	80.5	91.2	72.0
Task Arithmetic	77.4 (91.5)	1.19 (1.00)	68.8	55.2	78.7	89.8	83.7	79.1	91.5	72.4
Ties-Merging	77.5 (91.6)	1.19 (1.00)	68.3	56.3	79.4	89.8	83.7	79.4	91.6	71.2
Fine-tuned	84.6 (100)	1.25 (1.05)	69.1	82.7	85.5	90.9	84.0	84.4	92.9	87.4
SMILE	84.0 (99.3)	1.21 (1.02)	69.3	82.9	83.8	90.6	83.9	83.4	93.1	85.1
RanDeS-S (Ours)	83.9 (99.2)	1.20 (1.01)	69.2	79.0 ± 0.3	84.2	90.4	84.1	85.0	92.9	86.5
RanDeS-RSF (Ours)	83.0 (98.1)	1.20 (1.01)	69.1	81.3	82.2	90.5	83.2	79.1	92.7	85.6
RanDeS-SRSF (Ours)	84.4 (99.8)	1.20 (1.01)	69.1	82.7	85.0	90.9	83.8	84.2	92.7	86.9

5.9 Scalability Analysis

Our method scales effectively to merging larger models and more tasks, as demonstrated on CLIP ViT-L/14 with 8, 14, and 20 image classification tasks (Table 5). RanDeS-SRSF achieves near fine-tuned performance (93.5% vs 94.2% for 20 tasks) while maintaining constant 2.87GB storage regardless of task count. In contrast, the state-of-the-art model TALL-masks+TA [Wang et al., 2024] requires progressively more storage (5.42GB to 9.25GB) as tasks increase. Though Task Arithmetic uses only 1.59GB, its performance drops significantly with more tasks. Model retrieval remains efficient, requiring just 658.19ms per CLIP ViT-L/14 model on an Intel Xeon Gold 6448Y CPU.

6 Related Work

Model Merging. Recent research on model merging is largely founded on *linear mode connectivity (LMC)* [Frankle et al., 2020, Neyshabur et al., 2020], which posits that models fine-tuned from the same pre-trained model are connected by a linear path along which performance remains constant. Building upon this concept, Wortsman et al. [2022] and Li et al. [2024] demonstrated that a set of specialist models can be directly interpolated to obtain a multi-task model. Ilharco et al. [2022] proposed interpolating the parameter deltas (referred to as "task vectors") instead. However, these methods suffer from *task interference*: when different models adjust the same parameters in conflicting ways, summing these adjustments leads to interference and degraded performance on individual tasks [Yadav et al., 2024, Tang et al., 2024b, Wang et al., 2024]. To mitigate this interference, various strategies have been proposed. Yang et al. [2023] optimized the merging coefficients for different tasks and layers to reduce interference. Yadav et al. [2024] addressed the conflict by removing

Table 5: Performance and memory comparison of CLIP ViT-L/14 models across three test scenarios with 8, 14, and 20 image classification tasks, showing absolute and normalized accuracy (%), as well as memory footprint (Gb). Results averaged over three runs where applicable. Variances smaller than 0.1% are omitted.

Method	8 tasks		14 tasks		20 tasks	
	Acc.(%) \uparrow	Bits(Gb) \downarrow	Acc.(%) \uparrow	Bits(Gb) \downarrow	Acc.(%) \uparrow	Bits(Gb) \downarrow
Pre-trained	64.5 (68.3)	1.59 (1.00)	68.1 (72.8)	1.59 (1.00)	65.2 (69.2)	1.59 (1.00)
Task Arithmetic	84.0 (88.7)	1.59 (1.00)	79.1 (84.2)	1.59 (1.00)	73.8 (78.3)	1.59 (1.00)
Fine-tuned	94.4 (100)	10.53 (6.62)	93.5 (100)	18.18 (11.43)	94.2 (100)	25.84 (16.25)
Magnitude Masking	92.8 (98.2)	5.42 (3.41)	90.6 (96.7)	7.34 (4.62)	90.9 (96.4)	9.25 (5.82)
TALL Mask+TA	94.2 (99.7)	5.42 (3.41)	92.4 (98.8)	7.34 (4.62)	93.2 (98.9)	9.25 (5.82)
RanDeS-S (Ours)	93.0 (98.4)	<u>2.87 (1.81)</u>	88.8 (94.6)	<u>2.87 (1.81)</u>	87.1 \pm 0.1 (92.2)	<u>2.87 (1.81)</u>
RanDeS-RSF (Ours)	<u>94.2 (99.8)</u>	<u>2.87 (1.81)</u>	<u>92.8 (99.2)</u>	<u>2.87 (1.81)</u>	<u>93.4 (99.1)</u>	<u>2.87 (1.81)</u>
RanDeS-SRSF (Ours)	94.3 (99.9)	<u>2.87 (1.81)</u>	93.0 (99.5)	<u>2.87 (1.81)</u>	93.5 (99.3)	<u>2.87 (1.81)</u>

redundant parameters and resolving sign disagreements. Tang et al. [2024c] reduced interference by upscaling the multilayer perceptron (MLP) layers. Tang et al. [2024b] compressed task vectors using singular value decomposition (SVD) and performed routing between them to further diminish interference. Both Wang et al. [2024] and Yu et al. [2024] sparsified the task vectors to prevent task conflicts. Additionally, Ortiz-Jimenez et al. [2024] proposed fine-tuning the linearized model along the tangent space of the pre-trained model to promote weight disentanglement and avoid interference. In contrast to the above mentioned methods that aim to avoid conflicts, we intentionally accumulate interference among conflicting task vectors to facilitate their mutual cancellation.

Model Compression. Model compression techniques aim to reduce the memory footprint of models while maintaining their performance. Model pruning compresses neural networks by removing inessential parameters in either a structured [Anwar et al., 2017, Fang et al., 2023, He and Xiao, 2023, Wang et al., 2019] or unstructured [Liao et al., 2023, Kwon et al., 2020] manner. Parameter quantization saves memory and speeds up inference by converting the weights and activation values of a neural network from high precision to low precision [Gholami et al., 2022, Liu et al., 2021, Yuan et al., 2022]. Knowledge distillation reduces the memory footprint by training a smaller network to mimic a larger network’s behavior [Gou et al., 2021, Cho and Hariharan, 2019, Park et al., 2019, Zhao et al., 2022]. Leveraging the low-rank nature of model parameters, many works decompose weight matrices into low-rank matrices for memory reduction [Yu et al., 2017, Li et al., 2023, Guo et al., 2024]. Ryu et al. [2023] observed the low-rank nature of weight residuals in overparameterized models and proposed reducing storage demands for fine-tuned models through low-rank approximation of these residuals. Similarly, Tang et al. [2024b] compresses individual task vectors using SVD and routes through a set of them conditioned on input. Our work differs from these works in that we try to reduce redundancy across a set of aligned models rather than within them.

7 Discussion and Future Work

In this work, we introduce *RanDeS* as a principled framework to reduce interference in model merging frameworks, and two layer-wise efficient implementations. These data- and model-agnostic random operations enable users to i) efficiently modify the model merging combinations without the need for additional training or optimization; ii) merge additional models without increasing memory usage by saving random seeds. Evaluation on diverse model and task sets demonstrates that our method maintains high performance while keeping a constant memory footprint as more and larger models are merged. These attributes make our approach highly practical for real-world multi-model serving environments.

An interesting future direction is to further improve performance by increasing orthogonality, potentially through alternative random operations or more systematic approaches. Our method relies on specific properties of model parameters that emerge from fine-tuning. Identifying these properties and enhancing fine-tuning strategies could lead to better merging and compression performance. Since

we reduce cross-model redundancy, applying model compression algorithms could potentially further decrease memory footprint.

References

- Sajid Anwar, Kyuyeon Hwang, and Wonyong Sung. Structured pruning of deep convolutional neural networks. *ACM Journal on Emerging Technologies in Computing Systems (JETC)*, 13(3):1–18, 2017.
- Lukas Bossard, Matthieu Guillaumin, and Luc Van Gool. Food-101—mining discriminative components with random forests. In *Computer vision—ECCV 2014: 13th European conference, zurich, Switzerland, September 6–12, 2014, proceedings, part VI 13*, pages 446–461. Springer, 2014.
- Gong Cheng, Junwei Han, and Xiaoqiang Lu. Remote sensing image scene classification: Benchmark and state of the art. *Proceedings of the IEEE*, 105(10):1865–1883, 2017.
- Brian Cheung, Alexander Terekhov, Yubei Chen, Pulkit Agrawal, and Bruno Olshausen. Superposition of many models into one. *Advances in neural information processing systems*, 32, 2019.
- Jang Hyun Cho and Bharath Hariharan. On the efficacy of knowledge distillation. In *Proceedings of the IEEE/CVF international conference on computer vision*, pages 4794–4802, 2019.
- M. Cimpoi, S. Maji, I. Kokkinos, S. Mohamed, , and A. Vedaldi. Describing textures in the wild. In *Proceedings of the IEEE Conf. on Computer Vision and Pattern Recognition (CVPR)*, 2014.
- Tarin Clanuwat, Mikel Bober-Irizar, Asanobu Kitamoto, Alex Lamb, Kazuaki Yamamoto, and David Ha. Deep learning for classical japanese literature. *arXiv preprint arXiv:1812.01718*, 2018.
- Adam Coates, Andrew Ng, and Honglak Lee. An analysis of single-layer networks in unsupervised feature learning. In *Proceedings of the fourteenth international conference on artificial intelligence and statistics*, pages 215–223. JMLR Workshop and Conference Proceedings, 2011.
- Gregory Cohen, Saeed Afshar, Jonathan Tapson, and Andre Van Schaik. Emnist: Extending mnist to handwritten letters. In *2017 international joint conference on neural networks (IJCNN)*, pages 2921–2926. IEEE, 2017.
- Li Deng. The mnist database of handwritten digit images for machine learning research. *IEEE Signal Processing Magazine*, 29(6):141–142, 2012.
- Gongfan Fang, Xinyin Ma, Mingli Song, Michael Bi Mi, and Xinchao Wang. Depgraph: Towards any structural pruning. In *Proceedings of the IEEE/CVF conference on computer vision and pattern recognition*, pages 16091–16101, 2023.
- Jonathan Frankle, Gintare Karolina Dziugaite, Daniel Roy, and Michael Carbin. Linear mode connectivity and the lottery ticket hypothesis. In *International Conference on Machine Learning*, pages 3259–3269. PMLR, 2020.
- Amir Gholami, Sehoon Kim, Zhen Dong, Zhewei Yao, Michael W Mahoney, and Kurt Keutzer. A survey of quantization methods for efficient neural network inference. In *Low-Power Computer Vision*, pages 291–326. Chapman and Hall/CRC, 2022.
- Ian J Goodfellow, Dumitru Erhan, Pierre Luc Carrier, Aaron Courville, Mehdi Mirza, Ben Hamner, Will Cukierski, Yichuan Tang, David Thaler, Dong-Hyun Lee, et al. Challenges in representation learning: A report on three machine learning contests. In *Neural information processing: 20th international conference, ICONIP 2013, daegu, korea, november 3–7, 2013. Proceedings, Part III 20*, pages 117–124. Springer, 2013.
- Jianping Gou, Baosheng Yu, Stephen J Maybank, and Dacheng Tao. Knowledge distillation: A survey. *International Journal of Computer Vision*, 129(6):1789–1819, 2021.
- Yangyang Guo, Guangzhi Wang, and Mohan Kankanhalli. Pela: Learning parameter-efficient models with low-rank approximation. In *Proceedings of the IEEE/CVF Conference on Computer Vision and Pattern Recognition*, pages 15699–15709, 2024.

- Yang He and Lingao Xiao. Structured pruning for deep convolutional neural networks: A survey. *IEEE transactions on pattern analysis and machine intelligence*, 2023.
- Patrick Helber, Benjamin Bischke, Andreas Dengel, and Damian Borth. Eurosat: A novel dataset and deep learning benchmark for land use and land cover classification. *IEEE Journal of Selected Topics in Applied Earth Observations and Remote Sensing*, 12(7):2217–2226, 2019.
- Edward J Hu, Yelong Shen, Phillip Wallis, Zeyuan Allen-Zhu, Yuanzhi Li, Shean Wang, Lu Wang, and Weizhu Chen. Lora: Low-rank adaptation of large language models. *arXiv preprint arXiv:2106.09685*, 2021.
- Gabriel Ilharco, Marco Tulio Ribeiro, Mitchell Wortsman, Suchin Gururangan, Ludwig Schmidt, Hannaneh Hajishirzi, and Ali Farhadi. Editing models with task arithmetic. *arXiv preprint arXiv:2212.04089*, 2022.
- Xisen Jin, Xiang Ren, Daniel Preotiuc-Pietro, and Pengxiang Cheng. Dataless knowledge fusion by merging weights of language models. *arXiv preprint arXiv:2212.09849*, 2022.
- Jonathan Krause, Michael Stark, Jia Deng, and Li Fei-Fei. 3d object representations for fine-grained categorization. In *Proceedings of the IEEE international conference on computer vision workshops*, pages 554–561, 2013.
- Alex Krizhevsky. Learning multiple layers of features from tiny images. 2009. URL <https://api.semanticscholar.org/CorpusID:18268744>.
- Se Jung Kwon, Dongsoo Lee, Byeongwook Kim, Parichay Kapoor, Baeseong Park, and Gu-Yeon Wei. Structured compression by weight encryption for unstructured pruning and quantization. In *Proceedings of the IEEE/CVF Conference on Computer Vision and Pattern Recognition*, pages 1909–1918, 2020.
- Tao Li, Weisen Jiang, Fanghui Liu, Xiaolin Huang, and James T Kwok. Scalable learned model soup on a single gpu: An efficient subspace training strategy. *arXiv preprint arXiv:2407.03641*, 2024.
- Yixiao Li, Yifan Yu, Qingru Zhang, Chen Liang, Pengcheng He, Weizhu Chen, and Tuo Zhao. Lospars: Structured compression of large language models based on low-rank and sparse approximation. In *International Conference on Machine Learning*, pages 20336–20350. PMLR, 2023.
- Zhu Liao, Victor Quéru, Van-Tam Nguyen, and Enzo Tartaglione. Can unstructured pruning reduce the depth in deep neural networks? In *Proceedings of the IEEE/CVF International Conference on Computer Vision*, pages 1402–1406, 2023.
- James Liu, Guangxuan Xiao, Kai Li, Jason D Lee, Song Han, Tri Dao, and Tianle Cai. Bitdelta: Your fine-tune may only be worth one bit. *arXiv preprint arXiv:2402.10193*, 2024.
- Zhenhua Liu, Yunhe Wang, Kai Han, Wei Zhang, Siwei Ma, and Wen Gao. Post-training quantization for vision transformer. *Advances in Neural Information Processing Systems*, 34:28092–28103, 2021.
- Shayne Longpre, Le Hou, Tu Vu, Albert Webson, Hyung Won Chung, Yi Tay, Denny Zhou, Quoc V Le, Barret Zoph, Jason Wei, et al. The flan collection: Designing data and methods for effective instruction tuning. In *International Conference on Machine Learning*, pages 22631–22648. PMLR, 2023.
- Michael S Matena and Colin A Raffel. Merging models with fisher-weighted averaging. *Advances in Neural Information Processing Systems*, 35:17703–17716, 2022.
- Yuval Netzer, Tao Wang, Adam Coates, Alessandro Bissacco, Baolin Wu, Andrew Y Ng, et al. Reading digits in natural images with unsupervised feature learning. In *NIPS workshop on deep learning and unsupervised feature learning*, volume 2011, page 4. Granada, 2011.
- Behnam Neyshabur, Hanie Sedghi, and Chiyuan Zhang. What is being transferred in transfer learning? *Advances in neural information processing systems*, 33:512–523, 2020.

- Maria-Elena Nilsback and Andrew Zisserman. Automated flower classification over a large number of classes. In *2008 Sixth Indian conference on computer vision, graphics & image processing*, pages 722–729. IEEE, 2008.
- Guillermo Ortiz-Jimenez, Alessandro Favero, and Pascal Frossard. Task arithmetic in the tangent space: Improved editing of pre-trained models. *Advances in Neural Information Processing Systems*, 36, 2024.
- Wonpyo Park, Dongju Kim, Yan Lu, and Minsu Cho. Relational knowledge distillation. In *Proceedings of the IEEE/CVF conference on computer vision and pattern recognition*, pages 3967–3976, 2019.
- Omkar M Parkhi, Andrea Vedaldi, Andrew Zisserman, and CV Jawahar. Cats and dogs. In *2012 IEEE conference on computer vision and pattern recognition*, pages 3498–3505. IEEE, 2012.
- Bowen Ping, Shuo Wang, Hanqing Wang, Xu Han, Yuzhuang Xu, Yukun Yan, Yun Chen, Baobao Chang, Zhiyuan Liu, and Maosong Sun. Delta-come: Training-free delta-compression with mixed-precision for large language models. *arXiv preprint arXiv:2406.08903*, 2024.
- Alec Radford, Jeffrey Wu, Rewon Child, David Luan, Dario Amodei, Ilya Sutskever, et al. Language models are unsupervised multitask learners. *OpenAI blog*, 1(8):9, 2019.
- Alec Radford, Jong Wook Kim, Chris Hallacy, Aditya Ramesh, Gabriel Goh, Sandhini Agarwal, Girish Sastry, Amanda Askell, Pamela Mishkin, Jack Clark, et al. Learning transferable visual models from natural language supervision. In *International conference on machine learning*, pages 8748–8763. PMLR, 2021.
- Simo Ryu, Seunghyun Seo, and Jaejun Yoo. Efficient storage of fine-tuned models via low-rank approximation of weight residuals. *arXiv preprint arXiv:2305.18425*, 2023.
- Richard Socher, Alex Perelygin, Jean Wu, Jason Chuang, Christopher D Manning, Andrew Y Ng, and Christopher Potts. Recursive deep models for semantic compositionality over a sentiment treebank. In *Proceedings of the 2013 conference on empirical methods in natural language processing*, pages 1631–1642, 2013.
- Johannes Stal Kamp, Marc Schlippsing, Jan Salmen, and Christian Igel. Man vs. computer: Benchmarking machine learning algorithms for traffic sign recognition. *Neural networks*, 32:323–332, 2012.
- Anke Tang, Li Shen, Yong Luo, Han Hu, Bo Do, and Dacheng Tao. Fusionbench: A comprehensive benchmark of deep model fusion. *arXiv preprint arXiv:2406.03280*, 2024a.
- Anke Tang, Li Shen, Yong Luo, Shuai Xie, Han Hu, Lefei Zhang, Bo Du, and Dacheng Tao. Smile: Zero-shot sparse mixture of low-rank experts construction from pre-trained foundation models. *arXiv preprint arXiv:2408.10174*, 2024b.
- Anke Tang, Li Shen, Yong Luo, Nan Yin, Lefei Zhang, and Dacheng Tao. Merging multi-task models via weight-ensembling mixture of experts. *arXiv preprint arXiv:2402.00433*, 2024c.
- Bastiaan S Veeling, Jasper Linmans, Jim Winkens, Taco Cohen, and Max Welling. Rotation equivariant cnns for digital pathology. In *Medical Image Computing and Computer Assisted Intervention–MICCAI 2018: 21st International Conference, Granada, Spain, September 16–20, 2018, Proceedings, Part II 11*, pages 210–218. Springer, 2018.
- Pablo Villalobos, Jaime Sevilla, Tamay Besiroglu, Lennart Heim, Anson Ho, and Marius Hobbahn. Machine learning model sizes and the parameter gap. *arXiv preprint arXiv:2207.02852*, 2022.
- Alex Wang. Glue: A multi-task benchmark and analysis platform for natural language understanding. *arXiv preprint arXiv:1804.07461*, 2018.
- Ke Wang, Nikolaos Dimitriadis, Guillermo Ortiz-Jimenez, François Fleuret, and Pascal Frossard. Localizing task information for improved model merging and compression. *arXiv preprint arXiv:2405.07813*, 2024.

- Ziheng Wang, Jeremy Wohlwend, and Tao Lei. Structured pruning of large language models. *arXiv preprint arXiv:1910.04732*, 2019.
- Mitchell Wortsman, Gabriel Ilharco, Samir Ya Gadre, Rebecca Roelofs, Raphael Gontijo-Lopes, Ari S Morcos, Hongseok Namkoong, Ali Farhadi, Yair Carmon, Simon Kornblith, et al. Model soups: averaging weights of multiple fine-tuned models improves accuracy without increasing inference time. In *International conference on machine learning*, pages 23965–23998. PMLR, 2022.
- Han Xiao, Kashif Rasul, and Roland Vollgraf. Fashion-mnist: a novel image dataset for benchmarking machine learning algorithms. *arXiv preprint arXiv:1708.07747*, 2017.
- Jianxiong Xiao, James Hays, Krista A. Ehinger, Aude Oliva, and Antonio Torralba. Sun database: Large-scale scene recognition from abbey to zoo. In *2010 IEEE Computer Society Conference on Computer Vision and Pattern Recognition*, pages 3485–3492, 2010. doi: 10.1109/CVPR.2010.5539970.
- Prateek Yadav, Derek Tam, Leshem Choshen, Colin A Raffel, and Mohit Bansal. Ties-merging: Resolving interference when merging models. *Advances in Neural Information Processing Systems*, 36, 2024.
- Enneng Yang, Zhenyi Wang, Li Shen, Shiwei Liu, Guibing Guo, Xingwei Wang, and Dacheng Tao. Adamerger: Adaptive model merging for multi-task learning. *arXiv preprint arXiv:2310.02575*, 2023.
- Le Yu, Bowen Yu, Haiyang Yu, Fei Huang, and Yongbin Li. Language models are super mario: Absorbing abilities from homologous models as a free lunch. In *Forty-first International Conference on Machine Learning*, 2024.
- Xiyu Yu, Tongliang Liu, Xinchao Wang, and Dacheng Tao. On compressing deep models by low rank and sparse decomposition. In *Proceedings of the IEEE conference on computer vision and pattern recognition*, pages 7370–7379, 2017.
- Zhihang Yuan, Chenhao Xue, Yiqi Chen, Qiang Wu, and Guangyu Sun. Ptq4vit: Post-training quantization for vision transformers with twin uniform quantization. In *European conference on computer vision*, pages 191–207. Springer, 2022.
- Borui Zhao, Quan Cui, Renjie Song, Yiyu Qiu, and Jiajun Liang. Decoupled knowledge distillation. In *Proceedings of the IEEE/CVF Conference on computer vision and pattern recognition*, pages 11953–11962, 2022.

A Overview

In this appendix we present more information about the experiment settings and analysis that could not fit in the main paper. In Sec. B we present more details about the datasets, models, and baseline methods used in evaluation. In Sec. C we include additional analysis and results.

B Experiment Setup

This section provides detailed descriptions for the datasets, baselines, and model fine-tuning settings.

Datasets Details. Evaluation are performed on two sets of datasets with different type of tasks.

1. **Image Classification Datasets:** For image classification, following Ilharco et al. [2022], Tang et al. [2024a], Wang et al. [2024], we use twenty tasks from CLIP’s [Radford et al., 2021] test set: SUN397 [Xiao et al., 2010], Cars [Krause et al., 2013], RESISC45 [Cheng et al., 2017], EuroSAT [Helber et al., 2019], SVHN [Netzer et al., 2011], GTSRB [Stallkamp et al., 2012], MNIST [Deng, 2012], DTD [Cimpoi et al., 2014], CIFAR100 [Krizhevsky, 2009], STL10 [Coates et al., 2011], Flowers102 [Nilsback and Zisserman, 2008], OxfordIIITPet [Parkhi et al., 2012], PCAM [Veeling et al., 2018], FER2013 [Goodfellow et al., 2013], EMNIST [Cohen et al., 2017], CIFAR10 [Krizhevsky, 2009], Food101 [Bossard et al., 2014], FashionMNIST [Xiao et al., 2017], RenderedSST2 [Socher et al., 2013, Radford et al., 2019], and KMNIST [Clanuwat et al., 2018]. For experiments on K tasks, the first K datasets from this list are select.
2. **Text Classification and Generation Datasets:** For text classification and generation, following Tang et al. [2024a], we have in total eight tasks from the GLUE benchmark [Wang, 2018]: CoLA, MNLI, MRPC, QNLI, QQP, RTE, SST2, and STSB.

Baseline Details. Our experiments compare the following baselines and our methods:

- **Pre-trained:** Pre-trained model used across all tasks (performance lower bound).
- **Fine-tuned:** Individual fine-tuned models (performance upper bound).
- **Weight Averaging** [Wortsman et al., 2022]: Merge models by directly averaging their parameters.
- **Fisher Merging** [Matena and Raffel, 2022]: Fisher Merging uses the Fisher information as a weight for each parameter during weight averaging.
- **RegMean** [Jin et al., 2022]: RegMean introduces a constraint in model merging by minimizing the L2 distance between the merged model and each individual model.
- **Task Arithmetic** [Ilharco et al., 2022]: Task Arithmetic computes the delta parameters between fine-tuned models and the base model (known as "task vectors") and aggregates them before adding into a pre-trained model.
- **Ties-Merging** [Yadav et al., 2024]: Ties-Merging addresses task conflict issues found in Task Arithmetic by eliminating redundant parameters and resolving symbol conflicts.
- **Layer-wise AdaMerging** [Yang et al., 2023]: Layer-wise AdaMerging finds optimal merging coefficients for each layer of each task vector in Task Arithmetic using test-time adaptation.
- **WEMoE** [Tang et al., 2024c]: WEMoE only merges the layer norm and attention layers while keeping the multi-layer perceptron layers unmerged, with a router to dynamically allocate weights to each MLP conditioned on the input.
- **SMILE** [Tang et al., 2024b]: SMILE compresses task vectors with singular value decomposition (SVD). It then determines the routing weights based on the alignment between input and each low-rank matrix.
- **TALL-masks+TA** [Wang et al., 2024]: TALL-masks+TA finds a binary parameter mask for each task vector by finding task-specific parameters with values deviate a lot from the aggregated multi-task vector. The corresponding mask for each task is applied to the multi-task vector before adding to a pre-trained model.

- **Magnitude Masking** [Wang et al., 2024]: Magnitude Masking differ from TALL-masks in that it determines per-task masks by keeping the top k% of each task vector’s parameters.
- **RanDeS-S (Ours)**: *RanDeS-S* performs layer shuffling among the repetitive layers in each delta before merging them with Task Arithmetic.
- **RanDeS-RSF (Ours)**: *RanDeS-RSF* applies random column-wise sign flips to each layer in each delta in Task Arithmetic.
- **RanDeS-SRSF (Ours)**: *RanDeS-SRSF* combines layer shuffling and column-wise random sign flips.

Model Details. We utilize fine-tuned models from Tang et al. [2024a] and Wang et al. [2024]. Here we describe the experimental setup for fine-tuning these models.

- **CLIP-ViT-B/32 Models**: The CLIP-ViT-B/32 models are fine-tuned by Tang et al. [2024a]. The Adam optimizer is employed with a fixed learning rate of $1e^{-5}$ for a total of 4,000 training steps with the batch size of 32. The zero-shot classification layer is computed on-the-fly with a frozen text encoder.
- **CLIP-ViT-L/14 Models**: Different from CLIP-ViT-B/32 models, these models are fine-tuned by Wang et al. [2024] with the training procedure described in Ilharco et al. [2022]. The AdamW optimizer is employed with a fixed learning rate of $1e^{-5}$ for a total of 2,000 training steps with the batch size of 128, and a cosine annealing learning rate schedule with 200 warm-up steps. The zero-shot classification heads are pre-computed and freed during fine-tuning process, following Ilharco et al. [2022] and Ortiz-Jimenez et al. [2024].
- **GPT-2 Models**: These models are fine-tuned by Tang et al. [2024a] with a constant learning rate of $5e^{-5}$ for 3 epochs.
- **Flan-T5-base and LoRA Models**: These models come from Tang et al. [2024a], with unspecified fine-tuning settings.

Evaluation Metrics. We measure performance using average task accuracy and normalized accuracy (relative to Fine-tuned baseline). For STSB [Wang, 2018], we use Spearman’s correlation. Memory efficiency is evaluated by estimated memory footprint in Gb and normalized footprint (relative to Pre-trained baseline).

Default Experimental Setup. We use global random seeds 42, 43, 44 for three runs per experiment on random approaches. Each model’s specific seed is generated by adding its index to the global seed, and is used consistently for layer shuffling and binary diagonal matrices across target layers. Following Ilharco et al. [2022], we apply uniform merging coefficients across models, optimized via grid search on validation sets (10% of training data, max 1,000 samples [Wang et al., 2024]). The search space is 0.1, 0.2, \dots , 1.0, extended to 0.1, 0.2, \dots , 2.0 for Flan-T5-base LoRA experiments.

C Additional Analysis

C.1 GPT-2 Text Classification Experiments

We evaluate our proposed methods against established baselines by compressing seven independently trained GPT-2 models on text classification tasks. As shown in Table 6, both our *RanDeS* algorithms achieved significantly higher classification accuracy while doubling the memory footprint, consistent with the high performance on other benchmarks.

C.2 Dynamics between Layer Shuffling and Random Sign Flips

We investigate how varying layer shuffling and random sign flips parameters affects model performance. We test target layer skip rates of 1, 2, 3, 4, where only every k-th target layer within repetitive layer sets is shuffled and sign-flipped. We also introduce *layer shifting* – a deterministic alternative to shuffling that shifts layers one position deeper with wrap-around – to study how different decorrelation approaches affect performance.

Table 6: Performance and memory comparison of GPT-2 models across seven GLUE text classification tasks, showing absolute and normalized accuracy (%), as well as memory footprint (Gb). Results averaged over three runs where applicable. Variances smaller than 0.1% are omitted.

Method	Avg.(%) \uparrow	Bits(Gb) \downarrow	CoLA	MNLI	MRPC	QNLI	QQP	RTE	SST-2
Pre-trained	44.5 (54.3)	0.498 (1.00)	30.9	33.0	31.4	49.2	63.2	52.7	50.9
Weight Averaging	56.1 (63.3)	0.498 (1.00)	55.0	55.1	51.0	57.6	76.7	44.8	52.5
Fisher Merging	58.7 (64.7)	0.498 (1.00)	54.8	58.0	39.5	63.3	81.5	49.1	64.7
RegMean	68.8 (79.7)	0.498 (1.00)	61.7	70.4	65.4	69.7	78.8	56.0	79.7
Task Arithmetic	70.0 (85.4)	0.498 (1.00)	68.7	68.6	69.6	70.5	81.8	47.3	83.6
Ties-Merging	70.0 (82.4)	0.498 (1.00)	68.4	71.4	68.4	69.6	82.4	47.7	81.8
Fine-tuned	82.0 (100)	3.49 (7.00)	76.8	82.1	80.4	88.3	89.6	65.3	91.2
RanDeS-S (Ours)	76.7 (93.5)	0.997 (2.00)	71.6	80.3	73.9	85.8	88.5	47.5	89.3
RanDeS-RSF (Ours)	71.3 \pm 0.6 (87.0)	0.997 (2.00)	62.3 \pm 0.3	78.2	46.1 \pm 4	82.6	88.4	52.7	88.9
RanDeS-SRSF (Ours)	76.6 \pm 0.2 (93.4)	0.997 (2.00)	70.3 \pm 0.1	81.0	61.0 \pm 1.3	87.2	89.3	57.5 \pm 0.3	90.2

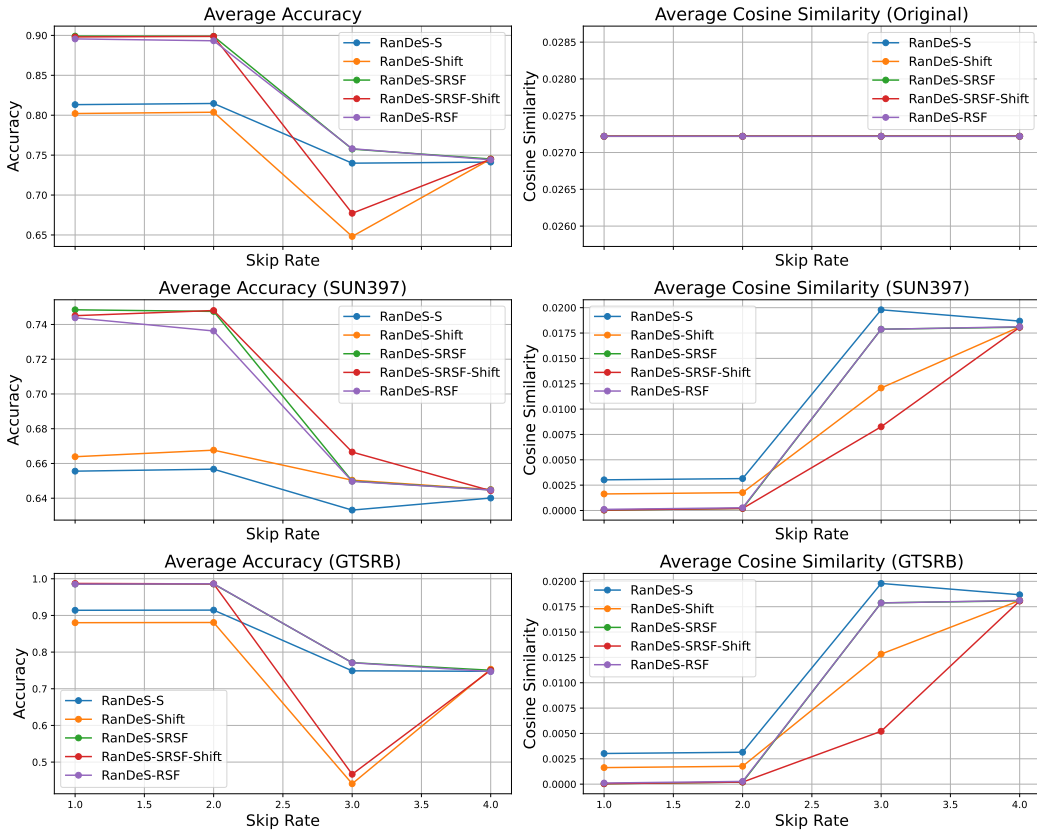


Figure 6: Average accuracy and cosine similarity among interfering deltas when retrieving SUN397 and GTSRB models from 8 merged CLIP-ViT-B/32 models with various target layer skipping rates and shuffling/superposition setups.

Experiments on eight CLIP-ViT-B/32 benchmarks (Figure 6) show averaged results across three repetitions, focusing on overall benchmark accuracy and two specific tasks: SUN397 [Xiao et al., 2010] and GTSRB [Stallkamp et al., 2012]. We analyze both task performance and average pairwise cosine similarity among deltas - both original and among interfering deltas during model retrieval.

As skip rate increases, accuracy declines while cosine similarity rises. Performance remains stable up to skip rate 2, suggesting potential memory savings through selective layer manipulation. For GTSRB, *RanDeS-S* outperforms *RanDeS-Shift* despite higher cosine similarity, indicating the method of achieving orthogonality matters beyond decorrelation levels. This pattern reverses for SUN397, revealing task-specific variations and opportunities for task-specific optimization.

The correlation between interfering deltas' cosine similarity and accuracy shows a negative trend (Figure 7), most pronounced in EuroSAT [Helber et al., 2019] and MNIST [Deng, 2012]. While patterns vary across tasks, peak accuracy consistently occurs near zero cosine similarity. This observation, combined with *RanDeS-SRSF*'s strong performance at low skip rates (Figure 6), suggests a cosine similarity threshold may exist above which method selection and task properties become less critical.

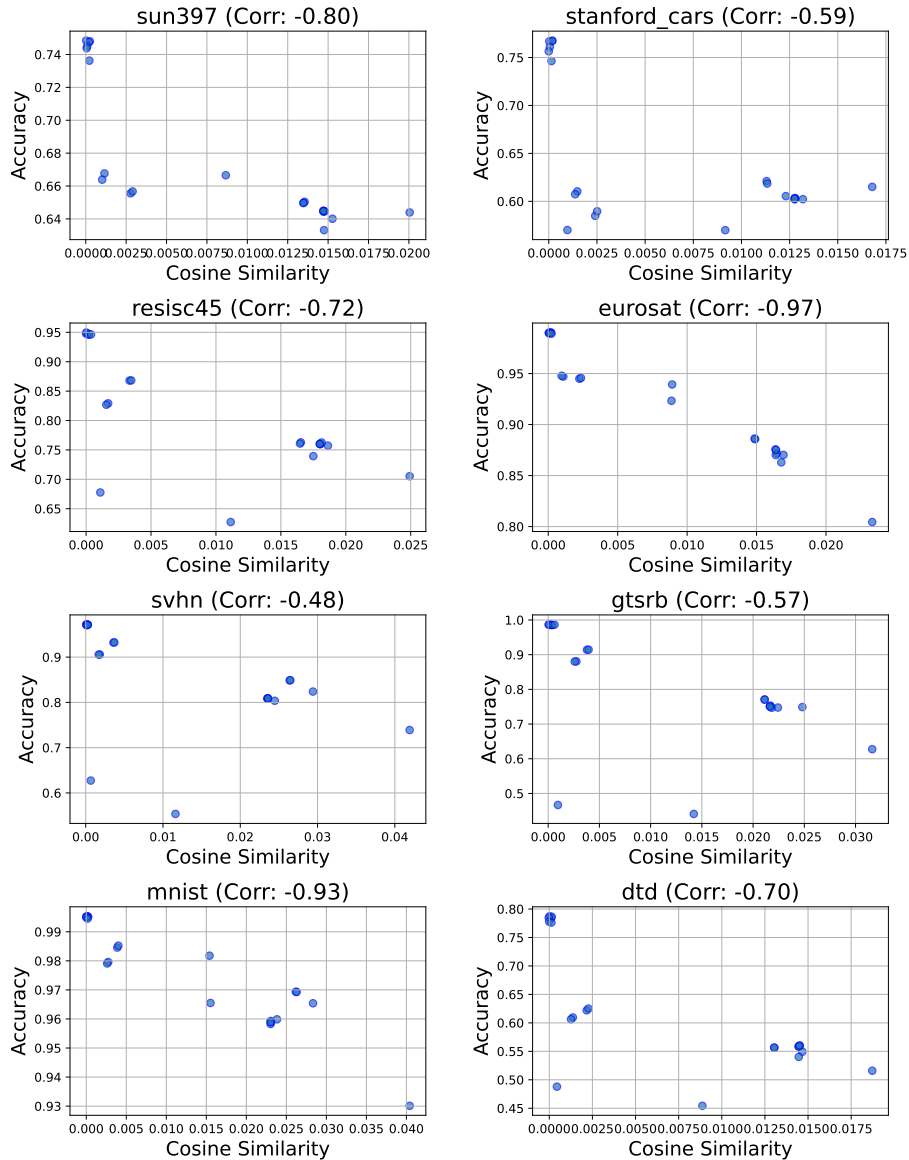


Figure 7: Correlation between the pairwise cosine similarity among interfering deltas and the accuracy on the eight image classification tasks, with CLIP-ViT-B/32 merged with different levels of shuffling and superposition.